Application of Fourier transform infrared spectroscopy to determine the reaction rate equation for cross-linking Matrimid 5218 with ethylenediamine in methanol

by

Kimberly Marie Yager

B.S., Wichita State University, 2013

A REPORT

submitted in partial fulfillment of the requirements for the degree

MASTER OF SCIENCE

Department of Chemical Engineering
College of Engineering

KANSAS STATE UNIVERSITY
Manhattan, Kansas

2018

Approved by:

Major Professor
John R Schlup

Copyright

Abstract

The cross-linking reaction of the polyimide Matrimid 5218 with ethylenediamine (EDA) in methanol was investigated using Fourier transform infrared (FTIR) spectroscopy. Peaks associated with breaking imide bonds and the formation of amide bonds were identified. Using an internal standard peak of 1014 cm^{-1} allowed for quantitative analysis to be applied. The peak areas, calculated by slice area, were used for absorbance ratio analysis to follow the cross-linking reaction as a function of time. Lastly, the absorbance values for the decreasing peak 1718 cm^{-1} were used to calculate the order of reaction for the reaction rate of the mechanism.

Table of Contents

List of Figures

List of Tables

List of Equations

Acknowledgements

I would like to acknowledge my immediate management, Larry Darbyshire and Lindsay Schurle, and executive management at Spirit AeroSystems, Inc. for supporting me in pursuing my Master of Science degree in Chemical Engineering and allowing me to use equipment at work for this report.

Also, I would like to acknowledge Dr. John R. Schlup, for without his guidance, this report would not be possible

Dedication

To my parents and Aaron, thank you for encouraging me to follow this dream and for not allowing me to become discouraged.

Chapter 1 - Introduction

Researchers have interest in polyimide (PI) membranes because they have a wide range of uses. Imide functional groups consist of a nitrogen sandwiched between a carbon-oxygen double bond on either side. They have been applied successfully in gas separation, pervaporation, and solvent resistant nanofiltration (Vanherck, et al., 2012). The reason PI membranes are so successful in these experiments is because they have mechanical stability and desirable thermal properties as well as chemical resistance to solvents (Tin, et al., 2003; Rahmani, et al., 2014). Gas separation is important because most natural gas has significant levels of carbon dioxide, which can lead to corrosion in factory operations. If the unwanted gas can be removed by passing through a polymer membrane, companies can save numerous costs. For gas separation, these types of membranes also show ideal selectivity of carbon dioxide over methane and high permeabilities (Rahmani, et al., 2015; Rahmani, et al., 2014). Even with these great qualities, researchers find that membrane properties could become even better by blending or cross-linking the polyimides.

By cross-linking the polyimides, covalent bonds form, stabilizing the molecules against thermal degradations (Nistor, et al., 2008). Plasticization, caused by CO_2, is a major problem with polymer membranes because it can minimize the performance of the membranes by reducing selectivity and decreasing gas separation capabilities. Cross-linking within the membranes helps decrease the effect of plasticization, which allows for better selectivity (Rahmani, et al., 2014). A disadvantage of polyimides is that they tend to swell in the presence of CO_2, but cross-linking minimizes the effect (Qiao & Chung, 2006).

The focus in this paper is the polyimide Matrimid 5218 (3,3'4,4'-benzophenonetetracarboxylic dianhydride (BTDA) and diamino-phenylindane). Matrimid PIs

have a greater selectivity towards CO_2 than CH_4 during gas separation (Rahmani, et al., 2014) as well as better gas permeability and a higher glass transition temperature (Nistor, et al., 2008) than other polyimides. Diamines are a popular choice as the crosslinking agent with Matrimid as they lead to improved CO_2 selectivity and minimizes the effect of aging on the thin membranes (Tin, et al., 2003; Powell, et al., 2007). These studies included the different diamine possibilities, p-xylenediamine (XDA) (Tin, et al., 2003), hexamethylenediamine (HMDA) (Rahmani, et al., 2014), and ethylenediamine (EDA) (Rahmani, et al., 2014; Stanford, et al., 2017) were used. EDA was the chosen cross-linking agent for the current study. Although both Rahmani, et al., (2014) and Stanford, et al., (2017) used EDA, Rahmani, et al., (2014) completed the cross-linking in liquid EDA, whereas Stanford, et al., (2017) used EDA vapor. Stanford, et al., (2017) chose to expose the Matrimid polyimide to EDA vapor rather than the liquid to reduce the swelling of the membrane and to not use another solvent.

The cross-linking reaction involves Matrimid 5218 (Figure. 1) being placed into a solution of EDA (Figure 2) in methanol. As the cross-linker reacts with the polymer membrane, the imide bonds break apart to form amide bonds (Figure 3). The amide functional group consists of a nitrogen atom attached to one carbon-oxygen double bond.

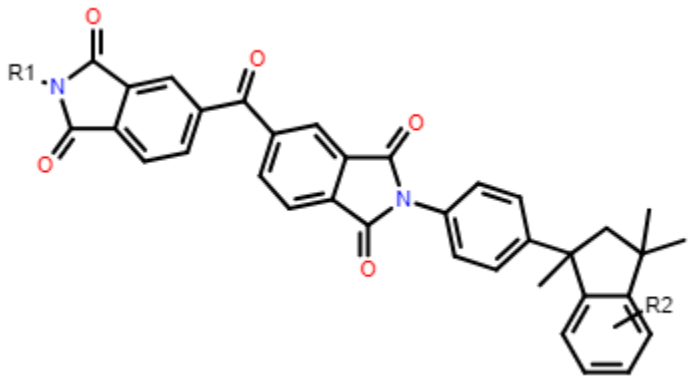

Figure 1. Chemical structure of Matrimid 5218.

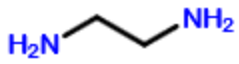

Figure 2. Chemical structure of ethylenediamine (EDA).

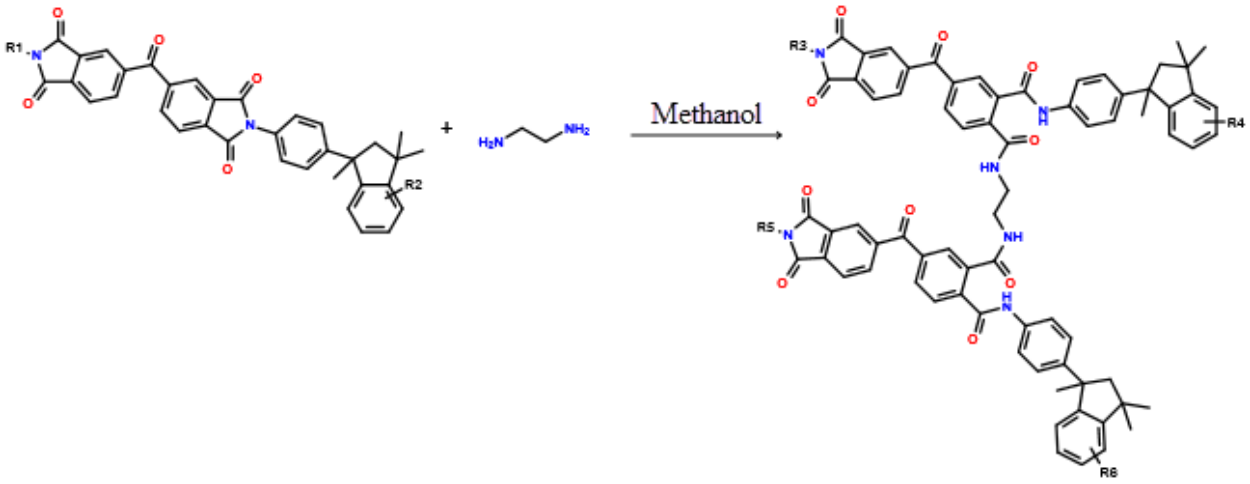

Figure 3. Chemical reaction of Matrimid 5218 and EDA in methanol.

Various methods have been used to characterize polyimide cross-linking mechanisms including differential scanning calorimetry (DSC) (Zhao, et al., 2008; Tin, et al., 2003), X-ray diffraction (XRD) (Chung, Shao, & Tin, 2006; Qiao & Chung, 2006), thermomechanical analysis (TMA) (Tin et al., 2003), thermogravimetric analysis (TGA) (Barsema, et al., 2004; Rahmani, et al., 2015), gel content (Zhao et al., 2008; Tin, et al., 2003), and dynamic mechanical analysis (DMA) (Tin, et al., 2003). The most frequent method researchers used to characterize cross-linking is Fourier transform infrared (FTIR) spectroscopy (Barsema, et al., 2004; Chung, Shao, & Tin, 2006; Qiao & Chung, 2006; Rahmani, et al., 2014, Rahmani, et al., 2015, Tin, et al., 2003; Zhao, et al., 2008).

Analysis by FTIR allows for the cross-linking mechanism to be confirmed. The peaks attributed to the imides in the original Matrimid polyimide decrease in intensity as the peaks for the forming amide bonds increase.

An FTIR attenuated total reflectance (ATR) accessory can be useful. An ATR accessory allows for easier sample preparation and reproducibility of spectra. The polymer membrane is placed directly onto a crystal with a higher refractive index than the sample. Zinc-selenium, germanium, and diamond crystals are popular choices with diamond being the best option because of its durability and chemical resistance. From those that employed FTIR-ATR (Zhao, et al., 2008; Chung, Shao, & Tin, 2006; Tin, et al., 2003; Qiao & Chung, 2006), researchers only used this technique to characterize the cross-linking. For the current study, FTIR-ATR data were used to determine the rate equation for the cross-linking reaction. With the lack of study into the rate of reaction, this information can lead to future research in this area for polymer cross-linking.

Chapter 2 - Experimental Setup

Sample Preparation

Dr. Wales, a research assistant for Dr. Rezac, prepared and provided the polyetherimide (PEI) samples. The asymmetric membranes were cast through a phase inversion process and then crosslinked. The crosslinking procedure started with a 5 wt% solution of ethylenediamine in 95 wt% methanol (both Fisher products). One membrane was held back as a control sample. The rest of the polymer membranes soaked in the solution for a specified amount of time (2, 4, 6, 8, and 18 hours) after which the membrane was removed and rinsed with methanol from a wash bottle. The polyimide was then placed in a jar of methanol for 30 minutes. After the 30 minutes, the polymer was taken out and rinsed with methanol from a wash bottle. The previous two steps were repeated, but the polymer was placed in a second jar with fresh methanol. After the last rinse of methanol, each membrane was left to dry at atmospheric conditions overnight.

Equipment Setup

For FTIR analysis of the PEI samples, a Thermo Scientific Nicolet iS50 FTIR spectrometer (Thermo Fisher, Madison, Wisconsin) with a diamond ATR crystal accessory was used to collect the spectra. Data were acquired and analyzed using OMNIC^{TM} version 9.2.98 software. The resolution was set to 4.000 wavenumbers, and 45 scans were averaged. A range from 400 to 4000 cm^{-1} wavenumbers was utilized in the spectra with an optical velocity of 0.4747 cm/s. The FTIR was equipped with a KBr beamsplitter and a deuterated triglycine sulfate (DTGS) detector. The gain was set to 4. The smaller the gain, the better the detector signal is amplified electronically. The aperture was set to 80, which controls the intensity of infrared that reaches the sample. Automatic atmospheric suppression was employed,

suppressing the effects of water vapor and carbon dioxide in the environment on the collected spectra over the wavenumber range.

Other advanced settings chosen were the zero filling level, apodization, and phase correction. Two levels of zero filling were the default option. The Norton-Beer strong (N-B strong) function was used to optimize the apodization (Naylor & Tahic, 2007). Phase correction was set to the Mertz algorithm, the normal setting, which is employed in calculating the phase-corrected spectrum.

Calibration of Instrument

The FTIR used is left on at all times, purged with nitrogen gas. Before running any samples, a ValPro Qualification test was completed to check the instrument performance. It takes the spectrum of a sample of the atmosphere and then a polystyrene calibration standard and compares those current results to the known wavenumbers obtained by the manufacturer to insure it is working correctly. After passing the qualification, a background sample was taken. A new background sample was taken every 120 minutes to ensure a current background spectrum.

Attainment of Spectrum

With the fragile nature of the membrane, they are easily cut with scissors. A piece of the membrane slightly bigger than the ATR crystal window was cut with scissors cleaned with isopropyl alcohol. Each PEI membrane has a smooth (dense) and rough (porous) side. The piece of polyimide was placed smooth side down over the diamond crystal, and the ATR arm

was tightened down until it clicked once. The force applied by the ATR arm was 267 Newtons. A sample was then collected.

Three samples were obtained from the smooth side of each membrane. Then one sample was taken from the rough side of each for comparison (Figure 4). No noticeable differences appeared between the smooth and rough side; thus the results in this paper were based on the smooth side for consistency.

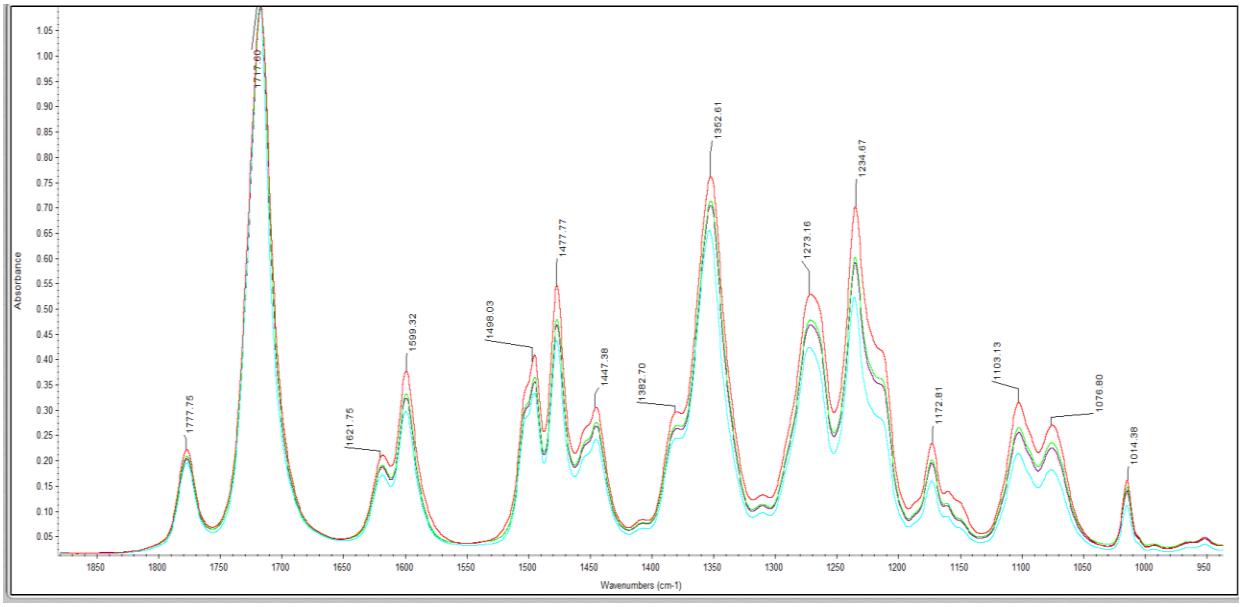

Figure 4. Comparison of smooth to rough side of membrane; from 1880 – 940 cm^{-1} for 0 hr. (no cross-linking) sample; Smooth side: red-sample 1; purple-sample 2; light green-sample 3; rough side: light blue-sample 1.

With the polymer membrane having two distinct sides, smooth and porous, an experiment was completed on a piece of fluorinated ethylene propylene (FEP) tubing that was found in the lab. The experiment was done to determine if differences in force would affect the signal by choosing different sides of the polymer membrane. Five replicate spectra were obtained from

the FEP tubing. It was determined that there was no effect on the signals attained based on force applied. Appendix A contains the data and spectra obtained during the experiment.

Chapter 3 - Results

Determination of Baseline Correction

Since the baselines of the spectra were not completely straight, two methods were considered to see if baseline correction yielded more accurate results: OMNIC^{TM} software's auto-baseline correction and manual correction. Any corrections to the baseline were made in absorbance mode versus transmittance because it is easier to observe the changes made as well as to determine the baseline points to employ with manual correction. The automatic baseline option takes the sloped baseline obtained and corrects it to the baseline points selected by the software for zero absorbance. The auto baseline adjustments can be altered to adjust the baseline further, but the default settings of a second-order polynomial and with 20 iterations were used. To correct the baseline manually, individual points were chosen along the baseline, which produced the new baseline. By picking points directly on the baseline, the point was moved to zero absorbance. A linear algorithm, the default option was chosen for the correction, which determines how the software calculates the values to correct the baseline. Figure 5 shows the comparison between the non-corrected, auto-baseline correction, and manual correction. From Figure 5, the non-corrected and auto baseline correction spectra are essentially the same, whereas the manual correction yielded lower absorbance units. Manual baseline was not the method chosen because there is the possibility of introducing fake peaks or other inaccuracies when choosing the individual points to zero out the baseline. The non-corrected baseline was chosen for simplicity.

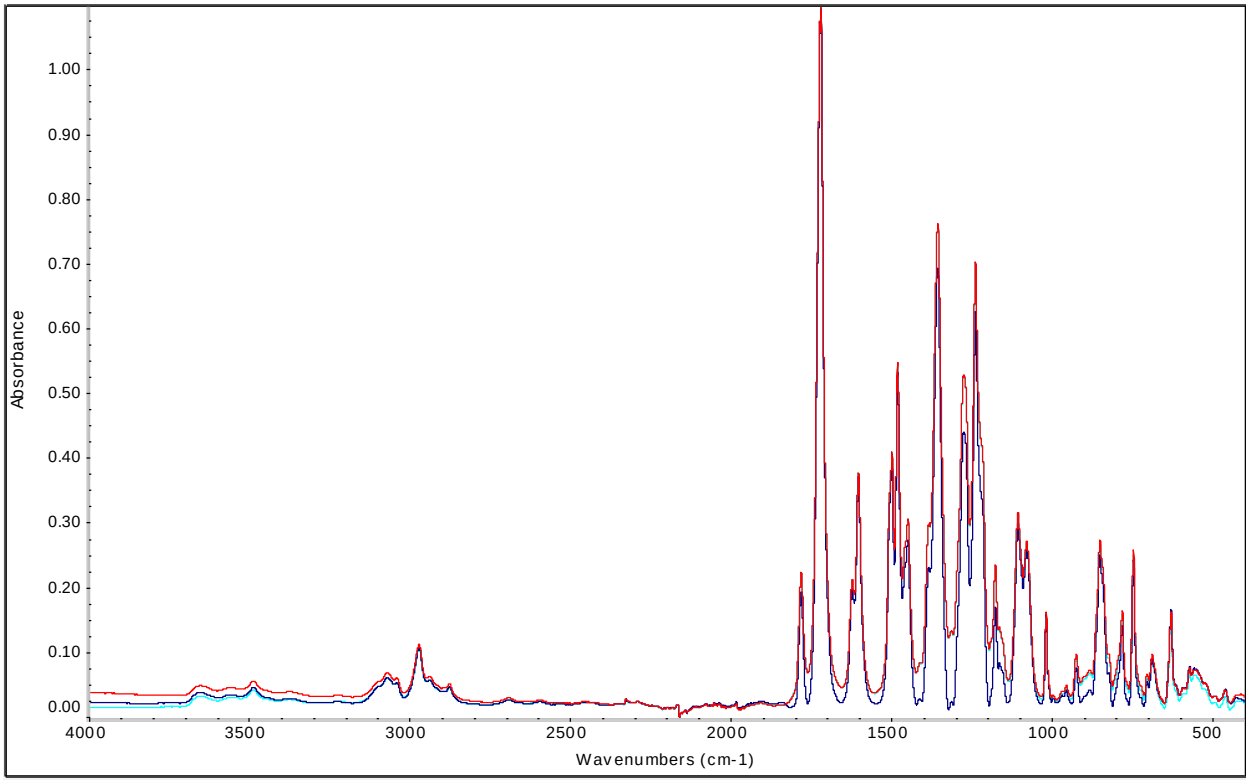

Figure 5. Comparison of non-corrected (red), auto-baseline correction (light blue), and manual baseline correction (navy blue) from 4000 – 490 cm^{-1} for the 0 hr. (no cross-linking) sample.

Identifying Peaks Associated with Cross-linking Reaction

Decreasing Peaks

Table 1 gives a description of the identified peaks for this mechanism from the literature.

As stated earlier, during the cross-linking process, certain peaks decrease because of the breaking of the imide bond to form an amide. Figure 6a and 6b compare the original polyimide with no cross-linking to the heavily crosslinked polymer, respectively. The peaks of interest which decrease are 1777, 1718, and 1352 cm^{-1}. The band at 1777 cm^{-1} corresponds to the asymmetric stretch of the carbon-oxygen double bond of the imide, while the peak at 1718 cm^{-1} is the symmetric stretch of the carbon-oxygen double bond of the imide. The band at 1352 cm^{-1} corresponds to the carbon-nitrogen stretch of the imide. The 1777 and 1718 cm^{-1} peaks were

chosen later for absorbance ratio analysis because they were peaks that were associated with the cyclic imide breaking apart to form the amide bond as well as the most isolated from other peak interference.

Increasing Peaks

As the cross-linking occurs, the imide functional group breaks apart to form amide bonds. The peaks associated with the amide bonds increase in absorbance with the peaks of particular importance occurring at 3291, 1637, and 1541 cm^{-1}. At 3291 cm^{-1}, the peak is the nitrogen-hydrogen stretching of the secondary amide formed. The band at 1637 cm^{-1} correlates to the carbon-oxygen double bond stretch of the amide, and the peak at 1541 cm^{-1} corresponds to the carbon-nitrogen stretch as well as the nitrogen-hydrogen deformation mode of the amide.

(a)

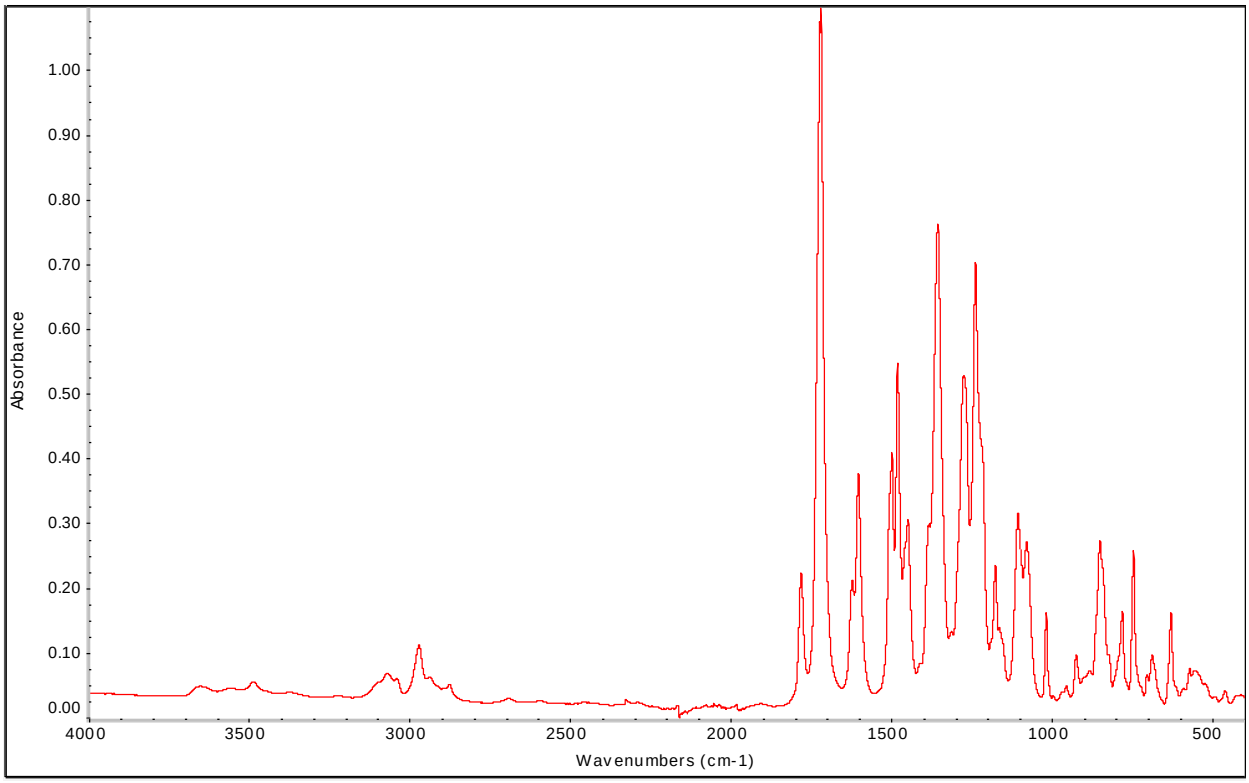

(b)

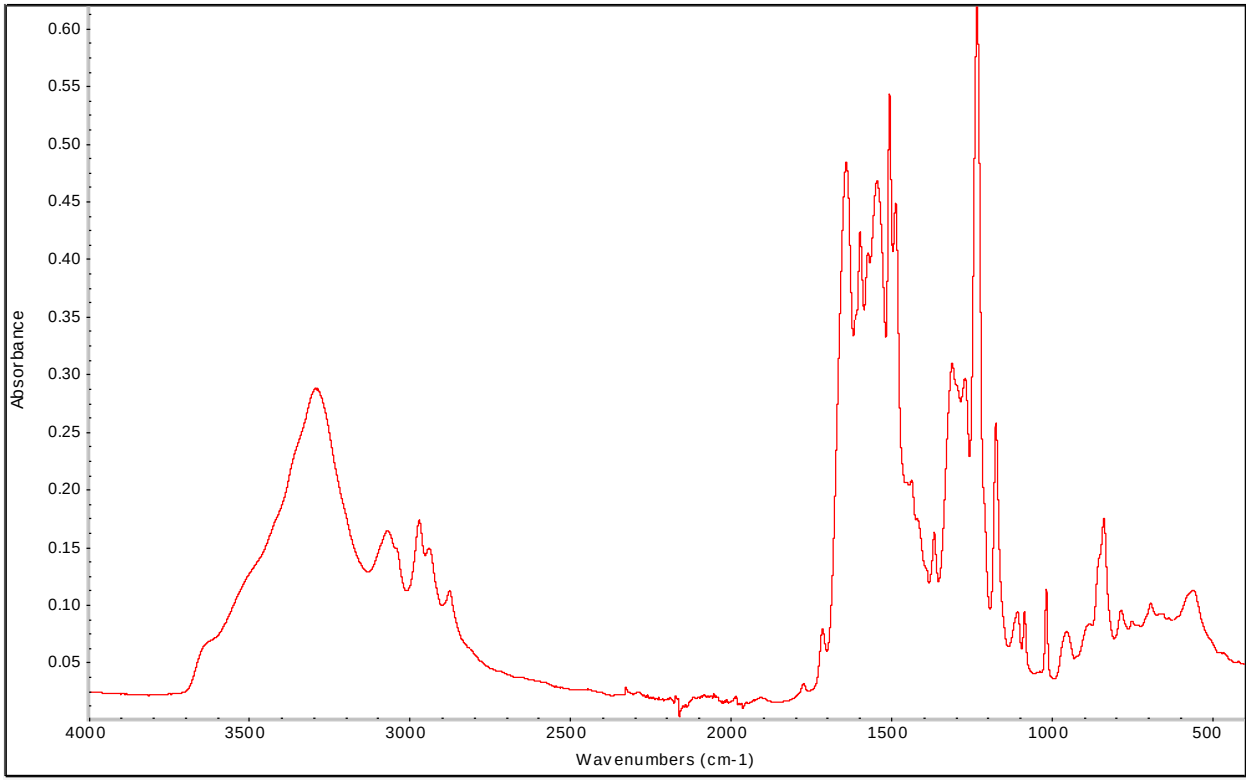

Figure 6. (a) Spectrum of 0 hr. with (no cross-linking) sample; (b) spectrum after 18 hr. cross-linking.

Peaks with No Change

Bonds that do not change during the cross-linking can serve as internal standards for later calculations. Bands that remained unchanged in absorbance were 2967, 1170, and 1014 cm^{-1}. The peak at 2967 cm^{-1} correlates to the carbon-hydrogen stretching of aliphatic methyl groups. At 1170 and 1014 cm^{-1} the bands are associated with the carbon-carbon double bond in-plane symmetric ring stretching of the 1,2,4-trisubstituted benzene ring.

Wavenumber (cm^{-1})	Description	Source
3483	N-H stretch primary amine end group	[1,13]
3291	N-H stretch secondary amide	[13,14]
3065	C-H stretch aromatic	[1,11]
3037	C-H stretch aromatic	[13]
2967	C-H stretch aliphatic methyl	[1,2,11,13]
2936	C-H stretch aliphatic methylene	[13]
2872	C-H stretch aliphatic methyl	[1,2,11,13]
1777	C=O asymmetric stretch imide	[1,4,10,11,14]
1718	C=O symmetric stretch imide	[2,10,11,13,14]
1637	C=O stretch of CONH (amide)	[4,10,11,13,14]
1618	C=C aromatic stretch	[1,13]
1595	C=C asymmetric ring IP ring stretch	[13]
1541	C-N stretch & N-H deformation (amide C-N-H group)	[4,10,13]
1501	C=C aromatic stretch	[1,2]
1478	C=C asymmetric ring IP ring stretch	[2,13]
1446	C-H methyl asymmetric deformation	[13]
1380	C-H methyl symmetric deformation	[13]
1352	C-N stretch imide	[4,10,11]
1232	C=C symmetric ring IP ring stretch	[13]
1170	C=C symmetric ring IP ring stretch	[13]
1014	C=C symmetric ring IP ring stretch	[13]
847	C-H aromatic OOP deformation (2 Hs)	[13]
835	C-H aromatic OOP deformation (2 Hs)	[13]

Table 1. Wavenumber and band descriptions.

Quantitative Analysis

Peak Area versus Peak Height

When deciding whether to use peak area or peak height for calculations, several factors were taken into consideration. In general, peak area has a larger signal-to-noise ratio than peak height. A larger signal to a smaller noise leads to more consistent values for quantitative calculations and better baseline corrections. Although peak heights may be used, peak areas are useful when the peaks change due to an increase in concentration. Peak areas also tend to be less sensitive to peak broadening due to diverse mechanisms. Peak areas were chosen herein to

calculate absorbance ratios for these reasons. Following the absorbance ratios will show how the decreasing peaks (1777 and 1718 cm^{-1}) change in comparison with the internal standard.

Baseline Evaluation

After the peak area was chosen as the method to obtain absorbance, the next decision was how to choose the baseline to calculate the areas. There were multiple options to evaluate the area including no baseline, single point baseline, two point baseline, and common tangent baseline. The two point baseline was chosen because it was the easiest method to obtain consistent results between each membrane sample. One point to the left and right on the baseline of each of the peaks of interest was chosen. These two wavenumbers were used for all six samples. If the peak had shifted to the left or right, two points close to the original two were chosen.

Slice Area

Slice area is a technique used to improve the accuracy of the results (McClure, 1987). It removes the summation of the area from the wings of the peak since that part of the peak tends to vary more with signal-to-noise ratios. The percentage of the absorbance to be included in the summation for the slice peak area is 30% of the peak intensity (McClure, 1987). That percentage is acceptable because anything under that number leads to uncertainty in the summation due to potential noise from the band. In the current study, 70% was used for slice area calculations because it allowed for good sampling of the peak to be clear of any interferences. Some signal-to-noise was given up, but the higher percentage optimized the data. For each peak, the max absorbance was found, then multiplied by 0.70 (Equation 1).

Equation 1.

$$\mathbf{70\%\ of\ Max\ Absorbance} = \boldsymbol{A_{max}} * \mathbf{0.70}$$

$$where\ A_{max}\ is\ the\ maximum\ absorbance\ of\ a\ peak$$

After this, the slice peak area was calculated using the Peak Area tool in the Omnic™ software. The slice area was calculated under the curve to the baseline using the seventy percent of the max absorbance values as the left and right limits. Figure 7 shows an example of how the slice area and baseline points were achieved using the 1014 cm^{-1} peak from one sample of the 0 hr. (no cross-linking membrane). Tables 2a, 2b, and 2c list the values obtained from calculating the average slice area of 3 replicates of the six membranes for each of the 1014, 1718, and 1777 cm^{-1} bands.

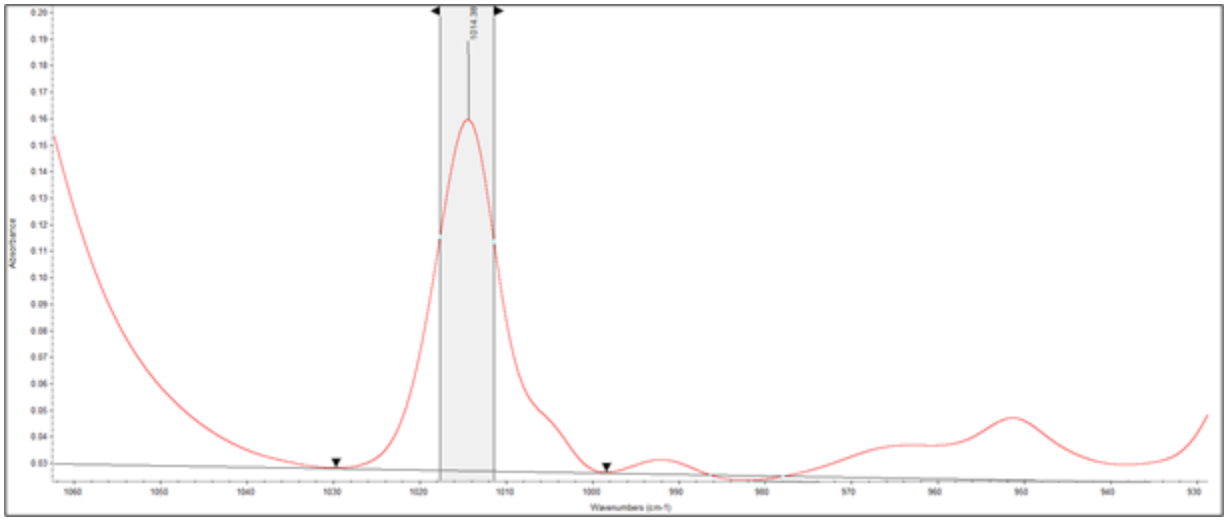

Figure 7. Slice peak area of 0 hr. (no cross-linking sample) of 1014 cm^{-1} peak.

a)

Sample	Avg. Max Absorbance	70% of Avg. Max Abs	Avg. Slice Area
0 hr	0.167	0.117	0.807
2 hr	0.154	0.108	0.709
4 hr	0.129	0.091	0.591
6 hr	0.17	0.119	0.741
8 hr	0.152	0.107	0.641
18 hr	0.119	0.083	0.532

b)

Sample	Avg. Max Absorbance	70% of Avg. Max Abs	Avg. Slice Area
0 hr	0.243	0.170	2.018
2 hr	0.174	0.122	1.464
4 hr	0.093	0.065	0.784
6 hr	0.098	0.069	0.784
8 hr	0.064	0.045	0.493
18 hr	0.026	0.018	0.131

c)

Sample	Avg. Max Absorbance	70% of Avg. Max Abs	Avg. Slice Area
0 hr	1.319	0.923	16.180
2 hr	0.846	0.592	10.896
4 hr	0.401	0.281	5.082
6 hr	0.384	0.269	4.689
8 hr	0.227	0.159	2.644
18 hr	0.077	0.054	0.437

Table 2. (a) Average slice peak area values for 1014 cm^{-1} peak; (b) average slice peak area values for 1718 cm^{-1} peak; (c) average slice peak area values for 1777 cm^{-1}.

Internal Standard Determination

An internal standard is used frequently in quantitative analysis. In this case, the internal standard was used to calculate the peak area ratios between it and two of the changing peaks. The three peaks, 2967, 1170, and 1014 cm^{-1}, that remained unchanged in absorbance were

compared to each other to find the best peak. Figure 8a and 8b shows the comparison of the 3 peaks in the 6 membrane samples.

First, each peak was considered in the context of neighboring peaks. The peak used for an internal standard should have a smooth curve with no shoulders and have local minima on either side that come close to the baseline of the spectra. When comparing the three peaks, the peaks at 2967 and 1170 cm^{-1} show interference with neighboring peaks and have shoulders that alter the peaks' baselines. The 1014 cm^{-1} peak has no shoulders and has distinct minima on either side, creating a nearly flat baseline.

(a)

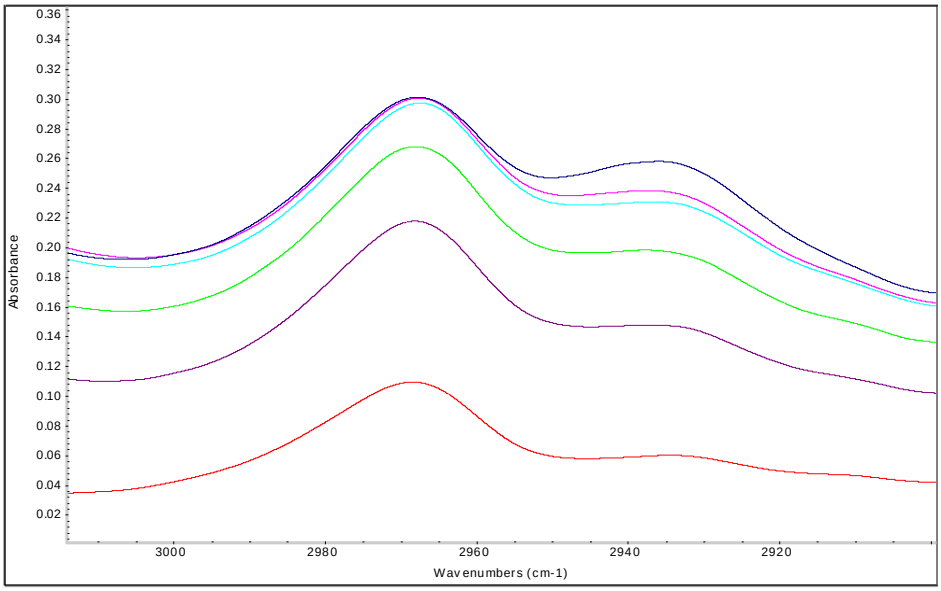

(b)

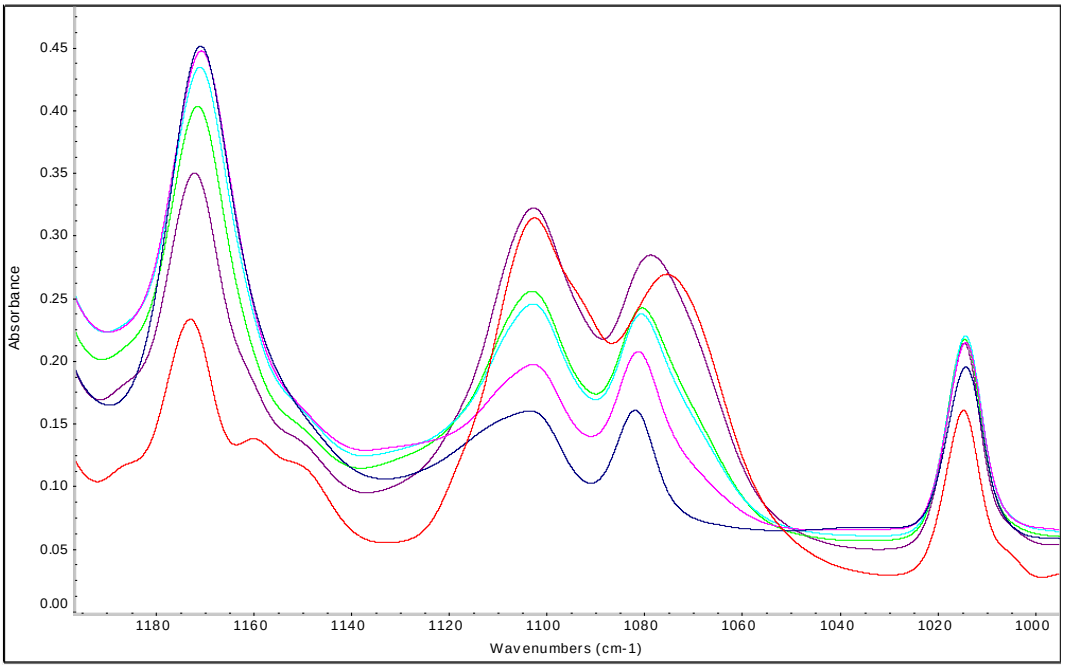

Figure 8. (a) No change peak 2967 cm^{-1}; (b) no change peaks 1170 and 1014 cm^{-1}; red: 0 hr. (no cross-linking); purple: 2 hr. cross-linking; light green: 4 hr. cross-linking; light blue: 6 hr. cross-linking; pink: 8 hr. cross-linking; navy blue: 18 hr. cross-linking.

Second, a more quantitative approach was taken. Slice peak areas were measured to see if one of the peaks had a more consistent area than the other two. Table 3 lists the slice area over the six samples for the 2967, 1170, and 1014 cm^{-1} peaks. The slice peak areas are plotted in Figure 9 for a better visual. From the graph, the 1170 cm^{-1} band's slice peak area changes the least during cross-linking. Although the 1170 cm^{-1} peak had more consistent slice peak areas, the 1014 cm^{-1} peak was chosen as the internal standard since it was more isolated in the spectrum and had a flatter baseline.

Slice Peak Area			
	1014 cm^{-1} peak	1170 cm^{-1} peak	2967 cm^{-1} peak
0 hr (no cross-linking)	0.724	0.896	0.852
2 hr	0.734	0.970	0.927
4 hr	0.612	0.864	0.791
6 hr	0.742	1.054	0.960
8 hr	0.650	0.956	0.830
18 hr	0.497	0.947	0.651

Table 3. Corrected slice peak areas for 1014, 1170, and 2967 cm^{-1} peaks.

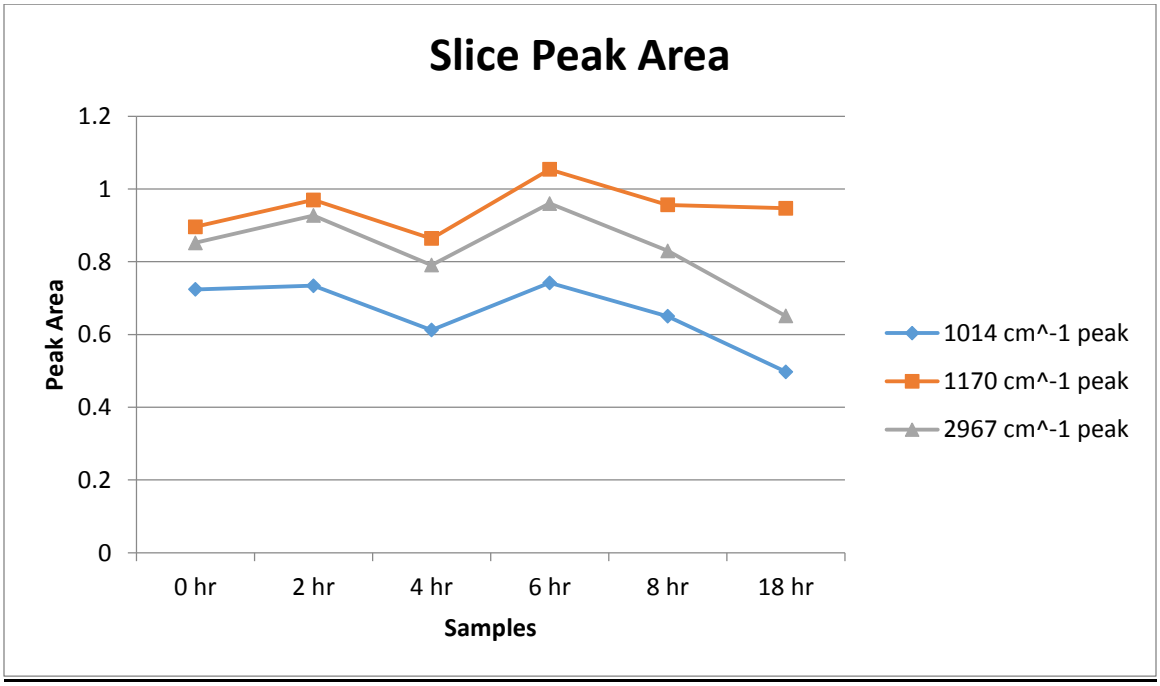

Figure 9. Graph of corrected slice peak areas for 1014, 1170, and 2967 cm^{-1} peaks.

Absorbance Ratio Analysis

Absorbance ratios were employed to follow the cross-linking as a function of time. Two decreasing peaks at 1777 and 1718 cm^{-1} were chosen to monitor the reaction and their ratio with the internal standard peak calculated. Equation 2 was used to calculate the slice peak area ratios.

Equation 2. $$\textit{Slice Peak Area ratio} = \frac{\textit{Area of Changing Peak}}{\textit{Area of Internal Std}}$$

The slice peak area values for all three peaks from the 6 samples were compiled together. The three replicates for each sample were averaged, and their standard deviations calculated (Table 4a). The individual replicates' slice peak areas were used to calculate the ratios in Table 4b. Figures 10a and 10b show that both the 1777 and 1718 cm^{-1} peaks decrease and that the carbon-oxygen double bond of the imide disappears more over time as cross-linking continues.

a)

Slice Peak Area						
	Internal Std		Changing peaks			
Sample	1014 cm^{-1} Avg.	Std Dev	1777 cm^{-1} Avg.	Std Dev	1718 cm^{-1} Avg.	Std Dev
0	0.807	0.071882	2.018	0.175184	16.180	1.878353
2	0.709	0.022189	1.464	0.035949	10.902	0.116715
4	0.591	0.022776	0.784	0.092781	5.082	0.554329
6	0.741	0.02203	0.784	0.100477	4.689	0.486967
8	0.641	0.010263	0.493	0.043841	2.644	0.359446
18	0.532	0.033922	0.131	0.010484	0.437	0.054945

b)

Ratios				
Sample	1777 cm^{-1} to 1014 cm^{-1} Avg.	Std Dev	1718 cm^{-1} to 1014 cm^{-1} Avg.	Std Dev
0	2.501	0.048	20.017	0.641
2	2.065	0.097	15.377	0.355
4	1.324	0.107	8.586	0.611
6	1.057	0.111	6.324	0.539
8	0.077	0.059	4.119	0.523
18	0.245	0.005	0.820	0.060

Table 4. (a) Slice peak areas of internal standard (1014 cm^{-1}) and changing peaks (1777 and 1718 cm^{-1}); (b) slice peak area ratios.

a)

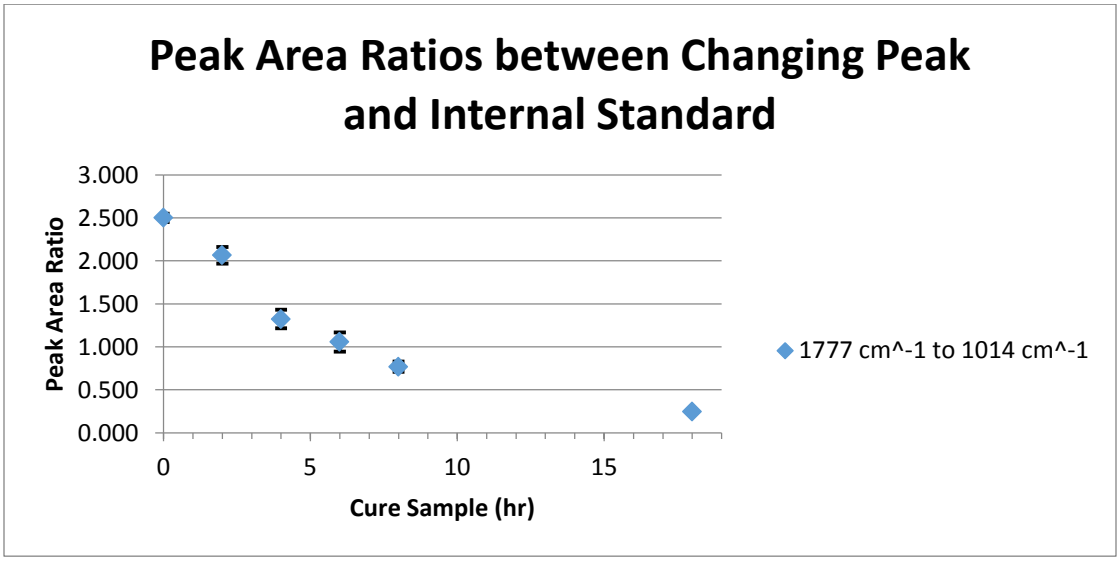

b)

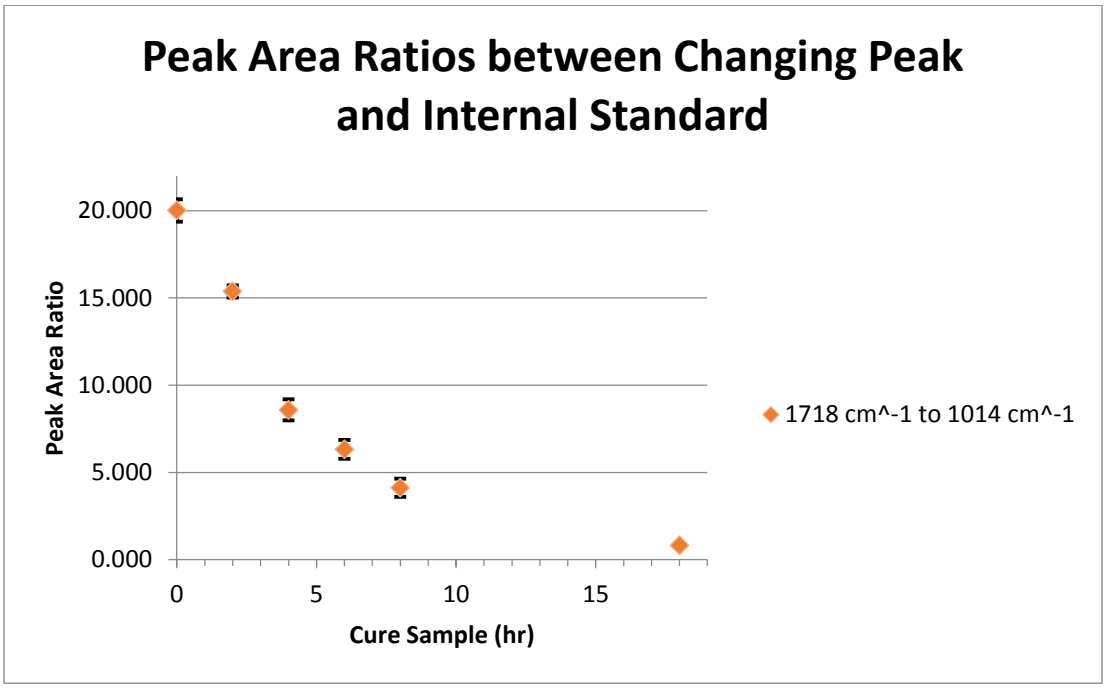

Figure 10. (a) Peak area ratios between 1777 and 1014 cm^{-1} peaks; (b) peak area ratios between 1718 and 1014 cm^{-1} peaks.; black error bars are one standard deviation.

Reaction Rate Equation

For the chemical reaction, Beer's Law (Equation 3) can be used to describe the linear relation of absorbance, A, in terms of concentration, C.

Equation 3. $$\boldsymbol{A = \varepsilon b C}$$

Pathlength determination is an issue with polymer membranes. However, ATR was used for analysis, which gives reproducible pathlengths and removes the uncertainty by passing through a thickness of a few microns. Since the pathlength, b, and the molar absorptivity, ε, are unknown, a ratio can be taken of Beer's Law in terms of the changing peak (sample) to the internal standard (reference), Equations 4 and 5, respectively.

Equation 4. $$A_{samp} = \varepsilon_{samp} b_{samp} C_{samp}$$

Equation 5. $$A_{ref} = \varepsilon_{ref} b_{ref} C_{ref}$$

By rearranging equations 4 and 5, an equation (Equation 6) for the ratio of sample concentration to the reference concentration, C_{samp}/C_{ref}, can be obtained.

Equation 6. $$\frac{C_{samp}}{C_{ref}} = \frac{A_{samp}}{A_{ref}} * \frac{\varepsilon_{ref} b_{ref}}{\varepsilon_{samp} b_{samp}}$$

A power rate law rate equation can be considered for this system (Equation 7).

Equation 7. $$-\frac{dC}{dt} = kC^n$$

Assuming A_{ref}, b_{samp}, b_{ref}, $\varepsilon_{samp}/\varepsilon_{ref}$, $\varepsilon_{ref}/\varepsilon_{samp}$ are constant, Equation 6 can be substituted for C in Equation 7 and rearranged as below.

Equation 8. $$-\frac{dA_{samp}}{dt} = BkA_{samp}^n$$

$$where\ B = \left(\frac{\varepsilon_{ref} b_{ref}}{\varepsilon_{samp} b_{samp} A_{ref}}\right)^n \left(\frac{A_{ref} \varepsilon_{samp} b_{samp}}{\varepsilon_{ref} b_{ref}}\right)$$

Now that the power rate law is in terms of absorbance, two different methods were used find the reaction order, n: differential and integral methods. The differential method of analysis is a graphical technique for interpreting the data. Taking the natural logarithm of both sides of Equation 8,

Equation 9. $$\ln\left(-\frac{dA_{samp}}{dt}\right) = [\ln(k) + \ln(B)] + n \ln(A_{samp})$$

where the equation is of the form y = b + mx. The data are compiled in Table 5. The slice area average for the 1718 cm^{-1} peak versus time (Figure 11) and the natural logarithm of $-dA_{samp}/dt$ versus the natural logarithm of A_{samp} (Figure 12) were plotted. A_{samp} is the slice area average of the 1718 cm^{-1} peak.

time (hr)	Slice Area Avg. (1718 cm^{-1})	-dAsamp/dt	ln(-dAsamp/dt)	ln(Asamp)
0	16.180	2.639	0.970	2.784
2	10.902	2.910	1.068	2.389
4	5.082	0.197	-1.627	1.626
6	4.689	1.023	0.022	1.545
8	2.644	0.221	-1.511	0.972
18	0.437			

Table 5. Differential method values.

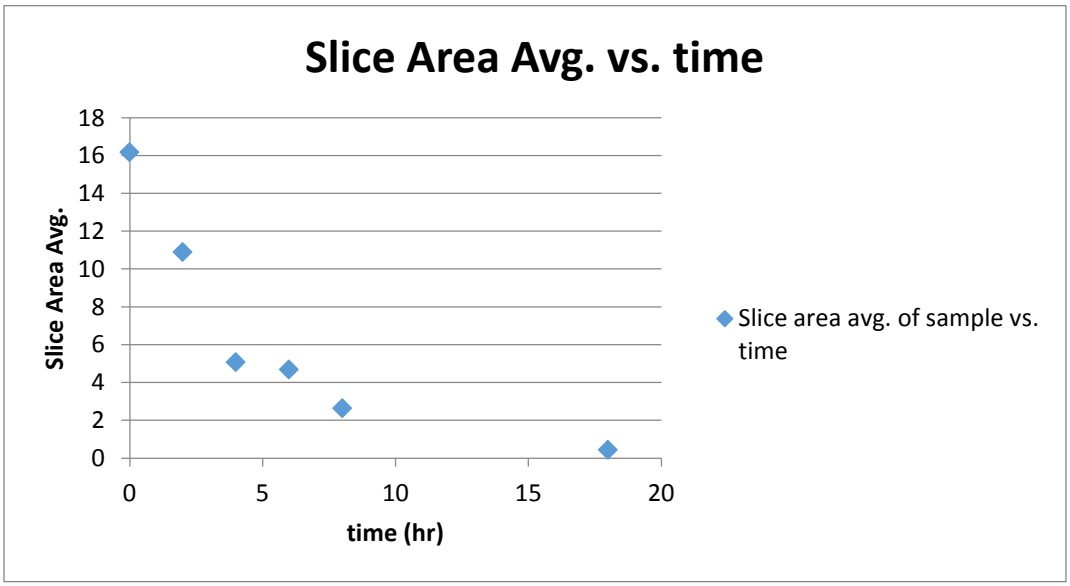

Figure 11. Slice area average for 1718 cm^{-1} peak versus time.

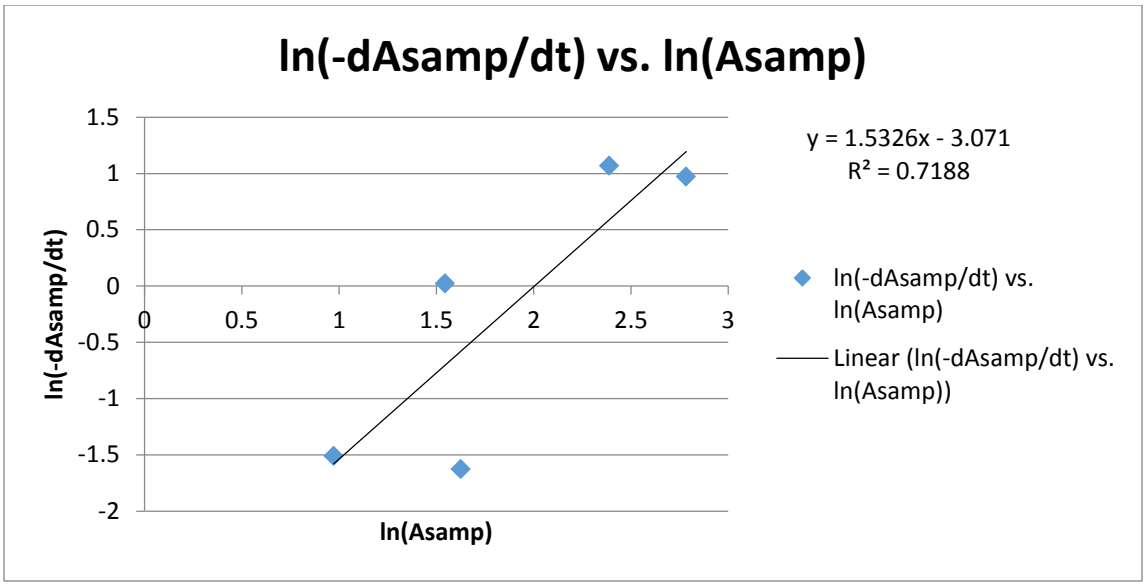

Figure 12. Differential method to determine reaction order, n.

The differential method determined a reaction order of 1.53 with a correlation coefficient of 0.7188. Using the LINEST statistical function in Microsoft Excel, the standard deviation for the reaction order and y-intercept were calculated. The reaction order with standard error is 1.53 ± 0.55 and the y-intercept is -3.07 ± 1.09.

The integral method is a trial-and-error method to find the reaction order. The reaction order is guessed until the resulting plot of data is linear with a correlation coefficient close to 1. Reaction orders of n = 0.5, 1, 1.5, and 2 were checked. Since the differential method calculated a reaction order of 1.53 ± 0.55, the data for n = 1 was of interest and is tabulated in Table 6 using Equations 10 and 11. The integral of both sides of Equation 8 were taken for calculations. Figure 13 shows the data plotted with a linear regression trendline. Table 7 compares the correlation coefficients of the four reaction orders checked. Appendix B gives the data, equations, and graphs plotted for n = 0.5, 1.5, and 2 that are not given here.

Slice Area Avg. ($1718\ cm^{-1}$)	time (hr)	$\ln(As_0)-\ln(As)$
16.180	0	0
10.902	2	0.395
5.082	4	1.158
4.689	6	1.239
2.644	8	1.811
0.437	18	3.612

Table 6. Integral method values for n=1.

Equation 10. $$-\int_{A_{samp_0}}^{A_{samp}} \frac{dA}{A} = \int_{t_0}^{t} Bkdt$$

Equation 11. $$\ln(A_{samp_0}) - \ln(A_{samp}) = Bkt$$

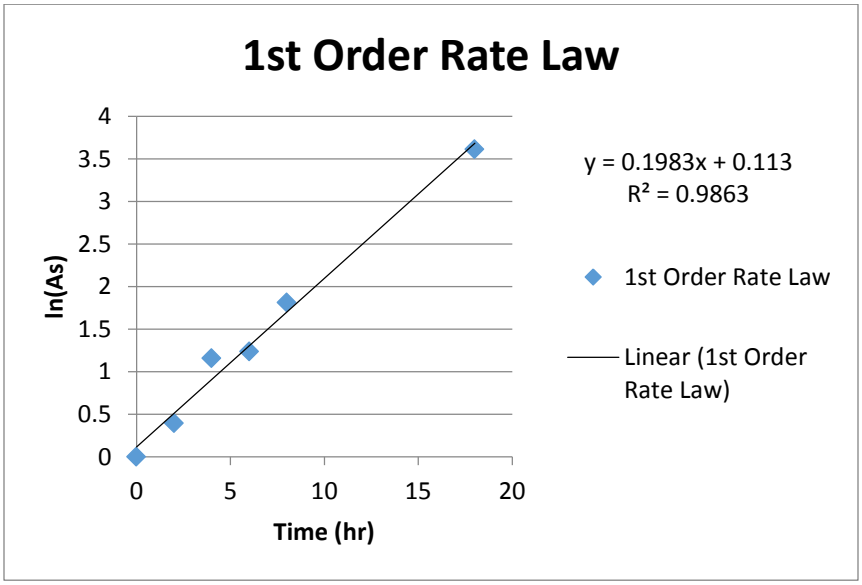

Figure 13. n = 1 order rate law by integral method.

Order of Rate Law (n)	Correlation Coefficient
0.5	0.8626
1	0.9863
1.5	0.9627
2	0.8902

Table 7. Comparison of correlation coefficients of different orders of the rate law.

A_s is the average slice area of the sample and A_{s0} is the average slice area of the sample at time 0 (0 hr. no cross-linking).

Looking at Table 7 for the integral method, the power rate law with the most linear regression line is where n = 1. It has a correlation coefficient of 0.9863. Standard deviations calculated from the LINEST function in Microsoft Excel were 0.1436 ± 0.014 for the slope and -0.2117 ± 0.122 for the y-intercept.

Comparing the differential method result of n = 1.53 to the integral method result of n = 1, the results came out close. Since the correlation coefficient for the integral method's results for n = 1 is the closest to 1, it fits the data the best. Looking at the differential method's result of n = 1.53, its standard deviation is 1.53 ± 0.55. The integral method's result of n = 1 would fall within this standard deviation, confirming the result. With the differential method, the reaction order has a larger standard deviation and smaller correlation coefficient than the integral method for n = 1. In the end, the integral method with a reaction order of 1 was chosen because of the better fit to the data.

Chapter 4 - Discussion

Looking at FTIR spectra from other papers, the data collected here are comparable. Several researchers documented the FTIR spectra of a pristine Matrimid 5218 membrane (Rahmani, et al., 2014; Rahmani, et al., 2015; Tin, et al., 2003). Of the three, Tin, et al. (2003) was the only one that stated the spectrum had come from an FTIR equipped with an ATR accessory. The three decreasing peaks (1777, 1718, 1352 cm^{-1}) are shown in each of the three papers, although the three decreasing peaks in this study most closely resemble the band wavenumbers of Tin, et al. (2003). This can most likely be attributed to the fact that Rahmani, et al. (2014) and Rahmani, et al. (2015) do not use an ATR accessory. For the cross-linked Matrimid with EDA, Rahmani, et al. (2014) shows a spectrum of this with a few small deviations from the one in Figure 6b. Rahmani, et al. (2014) uses EDA in methanol as the cross-linking agent but does so in a 10% (w/v) of solution instead of 5%. They also only expose the membrane to the cross-linking solution for 15 minutes versus hours in the current study. While there are small differences, the two increasing peaks from the formation of amide bonds (1637 and 1541 cm^{-1}) are shown in their spectrum with similar wavenumbers.

For the future, if more information was given with the membranes when they were received, the degree of cross-linking could have been calculated for the polymer reaction. It would have been interesting to see if there were any differences between the reaction rates orders of cross-linking if EDA was in vapor form versus liquid in methanol as used in this study. Stanford, et al. (2017) and Vanherck, et al. (2012) both use EDA vapor as an option for cross-linking. Thickness of the membranes affect the depth of cross-linking that occurs. Comparing different thicknesses during the same time of cross-linking would be intriguing to determine how much of the membrane is cross-linked. With other diamines (Rahmani, et al., 2014; Tin, et al.,

2003) and other reagents (Nistor, et al., 2008) as options for cross-linking, comparison of the different reaction rate orders would be interesting to see if they are the same or different.

Chapter 5 - Conclusion

In summary, this study explored the cross-linking of Matrimid 5218 with ethylenediamine (EDA) in methanol by using Fourier transform infrared (FTIR) spectroscopy to gather spectra and absorbance values to calculate the reaction order for the rate equation. Absorbance versus wavenumber spectra were compared with Rahmani, et al. (2014), Rahmani, et al. (2015), and Tin, et al. (2003). Decreasing peaks of 1777, 1718, and 1352 cm^{-1} and increasing peaks of 1637 and 1541 cm^{-1} found here were of similar wavenumbers to in the previously identified papers. By choosing a peak (1014 cm^{-1}) where its functional group assigned to the band did not change, an internal standard could be identified. This allowed for quantitative analysis of the data to find a reaction order of 1 for the rate equation. With other thermal techniques, the application of this data would be useful in finding out more information about the cross-linking mechanism.

Bibliography

1. Amooghin, A., Omidkhah, M., & Kargari, A. (2015). The effects of aminosilane grafting on NaY zeolite-Matrimid®5218 mixed matrix membranes for CO_2/CH_4 separation. *Journal of Membrane Science, 490,* 364-379.

2. Barsema, J.N., Klijnstra, S.D., Balster, J.H., van der Vegt, N.F.A, Koops, G.H., & Wessling, W. (2004). Intermediate polymer to carbon gas separation membranes based on Matrimid PI. *Journal of Membrane Science, 238,* 93-102.

3. Chung, T., Shao, L., & Tin, P. (2006). Surface modification of polyimide membranes by diamines for H_2 and CO_2 separation. *Macromol. Rapid Commun., 27,* 998-1003.

4. Dr. Wales. (2017, March 17). Personal Communication.

5. McClure, G.L. (1987). Quantitative analysis from the infrared spectrum. In H.A. Willis, J.H. van der Maas, & R.G.J Miller (3rd Ed.), *Laboratory Methods in Vibrational Spectroscopy* (pp. 145-201). New York, John Wiley & Sons Ltd.

6. Naylor, D., & Tahic, M. (2007). Apodizing functions for Fourier transform spectroscopy. *J. Opt. Soc. Am. A, 24(11),* 3644-3648.

7. Nistor, C., Shishatskiy, S., Popa, M., & Nunes, S.P. (2008). Composite membranes with cross-linked Matrimid selective layer for gas separation. *Environmental Engineering and Management Journal, 7(6),* 653-659.

8. Powell, C., Duthie, X., Kentish, S., Qiao, G., & Stevens, G. (2007). Reversible diamine cross-linking of polyimide membranes. *Journal of Membrane Science, 291,* 199-209.

9. Qiao, X., & Chung, T. (2006). Diamine Modification of P84 polyimide membanes for pervaporation dehydration of isopropanol. *AIChE Journal, 52(10),* 3462-3472.

10. Rahmani, M.R., Kazemi, A., Talebnia, F., & Khanbabaei, G. (2014). Preparation and characterization of cross-linked Matrimid membranes for CO_2/CH_4 separation. *Polymer Science, Ser. B, 56(5),* 650-656.

11. Rahmani, M., Kazemi, A., & Talebnia, F. (2015). Matrimid mixed matrix membranes for enhanced CO_2/CH_4 separation. *J. of Polym Eng,* 1-13.

12. Stanford, J.P., Pfromm, P.H., & Rezac, M.E. (2017). Effect of vapor phase ethylenediamine cross-linking of Matrimid on alcohol vapor sorption and diffusion. *Journal of Applied Polymer Science. 134(27).*

13. Thermo Fisher Scientific. Practical techniques for infrared spectral interpretation training manual. *300000-10001 Rev. B.*

14. Tin, P.S., Chung, T.S., Liu, Y., Wang, R., Liu, S.L, & Pramoda, K.P. (2003). Effects of cross-linking modification on gas separation performance of Matrimid membranes. *Journal of Membrane Science, 225,* 77-90.

15. Vanherck, K., Koeckelberghs, G., & Vankelecom, I.F.G. (2012). Crosslinking polyimides for membrane applications: A review. *Prog Polym Sci,* 1-23.

16. Zhao, H., Cao, Y., Ding, X., Zhou, M., & Yuan, Q. (2008). Effects of cross-linkers with different molecular weights in cross-linked Matrimid 5218 and test temperature on gas transport properties. *Journal of Membrane Science, 323,* 176-184.

Appendix A - FEP Tubing Force Experiment

A side experiment was completed to determine if force differences, from the smooth side to the porous side of the membrane, would affect the signal. FEP plastic tubing was cut in half by length, and five replicates were obtained from the outside and inside of the tubing. Spectra had non-corrected baselines and used an average of 45 frames to obtain the signal. Table 8 gives the absorbance values for two different peaks, 1201 and 1147 cm^{-1}. Figure 14 plots the absorbance values on a graph.

	Wavenumber (cm^{-1})	
	1201	1147
Replicate	**Absorbance**	
1	0.871	1.239
2	0.863	1.215
3	0.880	1.294
4	0.879	1.274
5	0.875	1.298

Table 8. Absorbance values from FEP tubing at 1201 and 1147 cm^{-1} peaks.

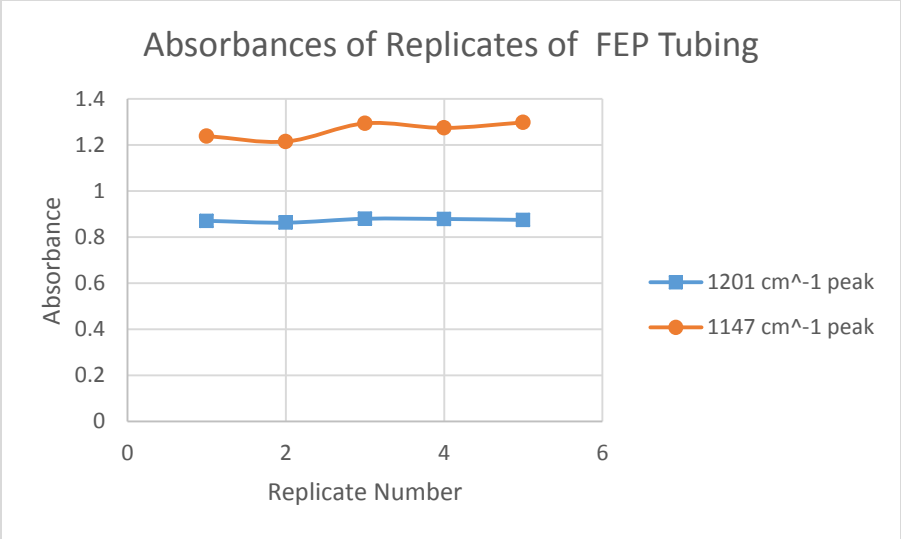

Figure 14. Comparison of FEP replicate samples' absorbances of 1201 and 1147 cm^{-1} peaks.

Figure 15 shows the full FTIR spectra of tubing, and Figure 16 shows a close-up of the spectra to show the two peaks used to obtain absorbance values.

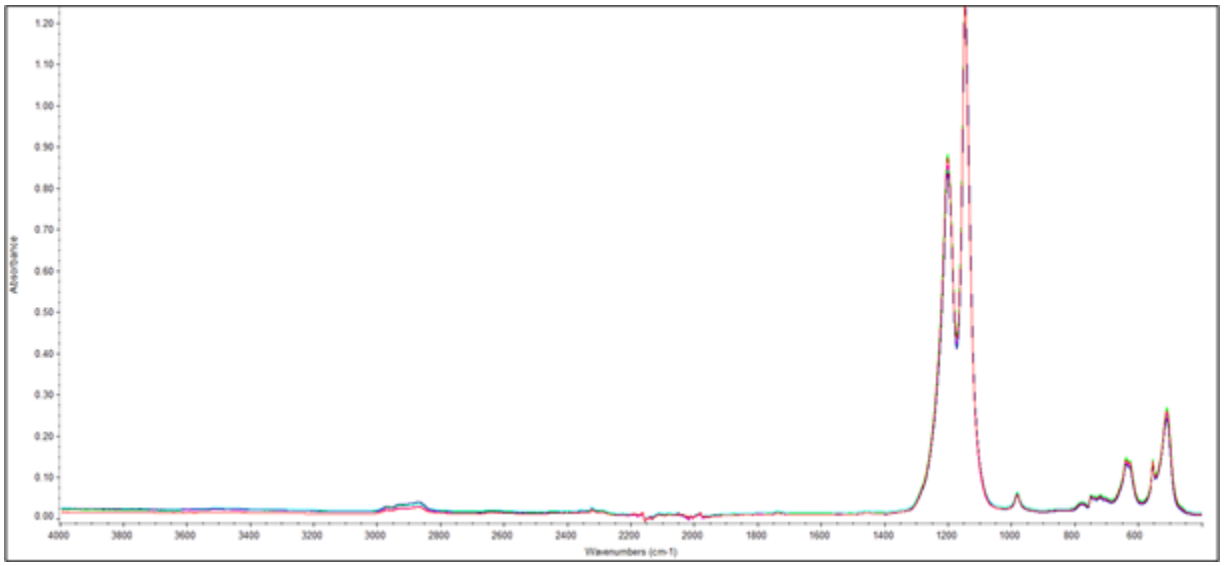

Figure 15. Full FTIR spectrum of FEP tubing from 4000 – 490 cm^{-1}; red: sample 1; light green: sample 2; light blue: sample 3; pink: sample 4; navy blue: sample 5.

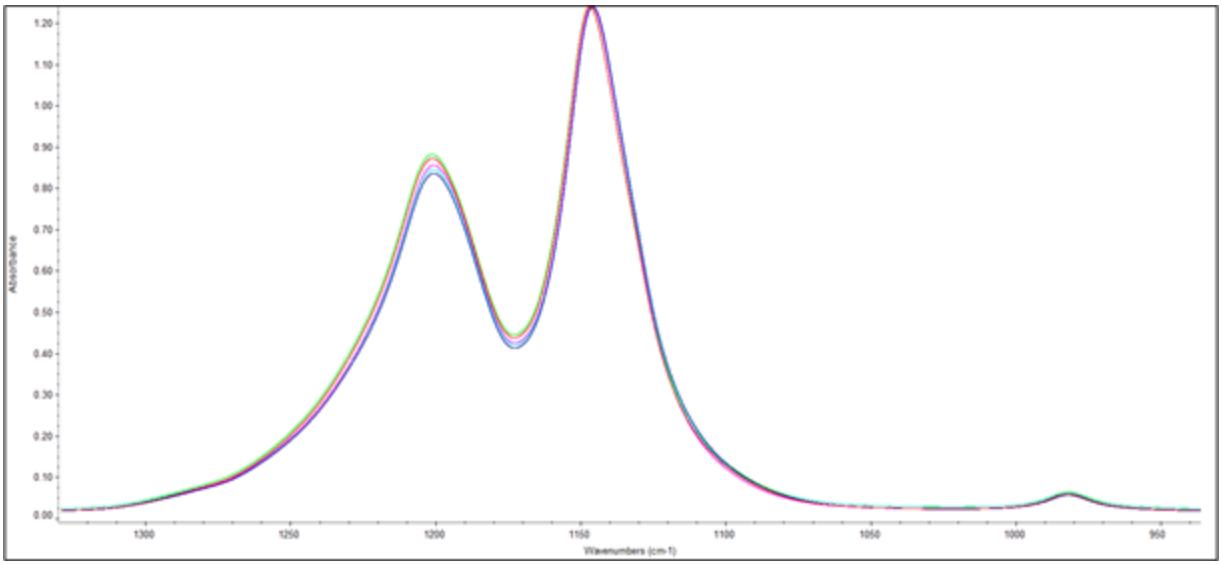

Figure 16. Close-up of the two peaks of interest, 1201 and 1147 cm^{-1}, from FEP tubing spectra from 1310 – 940 cm^{-1}; red: sample 1; light green: sample 2; light blue: sample 3; pink: sample 4; navy blue: sample 5.

Appendix B - Integral Method Data for n = 0.5, 1.5, and 2

Table 9 shows the data calculated for the reaction orders of n = 0.5, 1.5, and 2. Equations 12 and 13 were used for calculating n = 0.5, Equations 14 and 15 for n = 1.5 and Equations 16 and 17 for n = 2. Figures 17-19 shows the data plotted with linear trendlines and their correlation coefficients.

Slice Area Avg. (1718 cm^-1)	time (hr)	1/As	$1/As_0$	1/As-$1/As_0$	$2*As^{0.5}$	$2*As_0^{0.5}$	$2*As_0^{0.5}$-$2*As^{0.5}$	$2/As^{0.5}$	$2/As_0^{0.5}$	$2/As^{0.5}$-$2/As_0^{0.5}$
16.180	0	0.062	0.062	0	8.045	8.045	0	0.497	0.497	0
10.902	2	0.092		0.030	6.604		1.441	0.606		0.109
5.082	4	0.197		0.135	4.509		3.536	0.887		0.390
4.689	6	0.213		0.151	4.331		3.714	0.924		0.426
2.644	8	0.378		0.316	3.252		4.793	1.230		0.733
0.437	18	2.288		2.227	1.322		6.723	3.025		2.528

Table 9. Integral method values for n = 0.5, 1.5, and 2.

Equation 12. $$-\int_{A_{samp_0}}^{A_{samp}} \frac{dA}{\sqrt{A}} = \int_{t_0}^{t} Bkdt$$

Equation 13. $$2\sqrt{A_{samp_0}} - 2\sqrt{A_{samp}} = Bkt$$

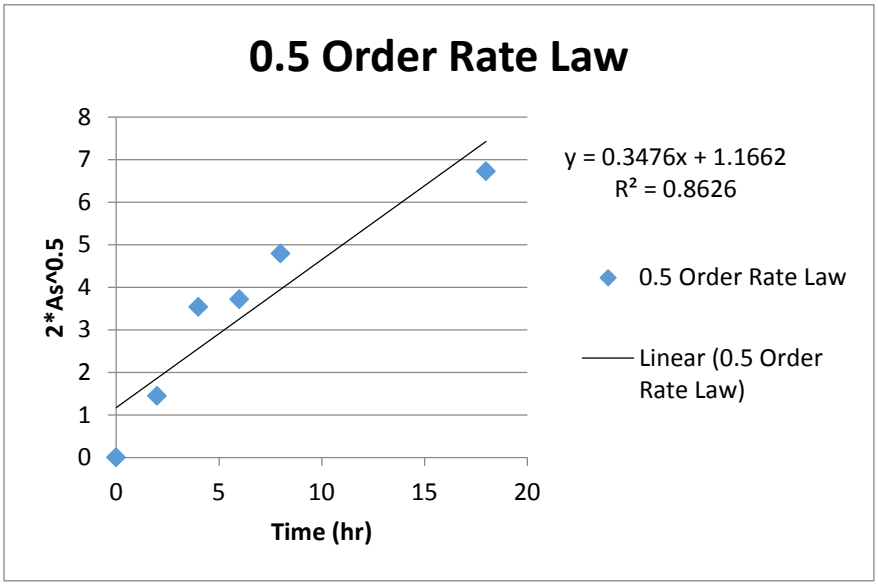

Figure 17. n = 0.5 order rate law by integral method.

Equation 14.

$$-\int_{A_{samp_0}}^{A_{samp}} \frac{dA}{A^{1.5}} = \int_{t_0}^{t} Bkdt$$

Equation 15.

$$\frac{2}{\sqrt{A_{samp}}} - \frac{2}{\sqrt{A_{samp_0}}} = Bkt$$

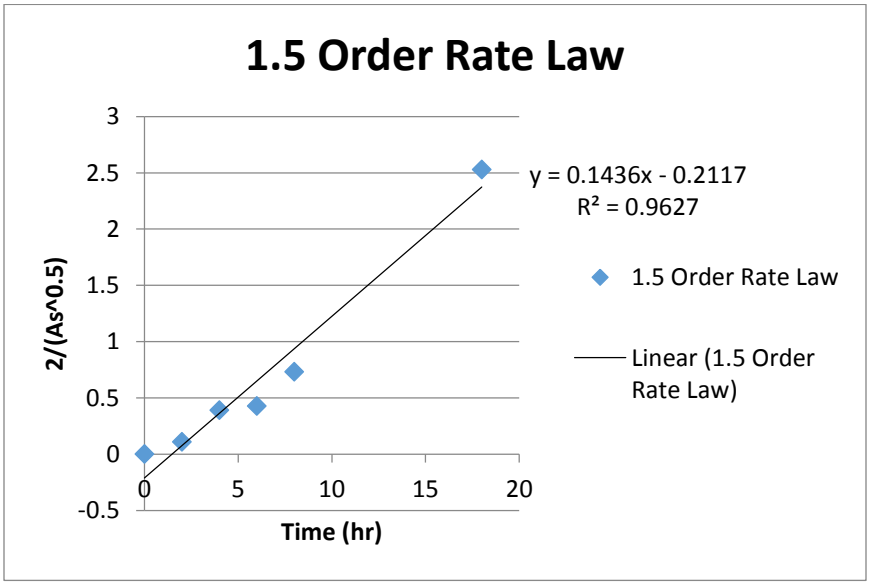

Figure 18. n = 1.5 order rate law by integral method.

Equation 16.

$$-\int_{A_{samp_0}}^{A_{samp}} \frac{dA}{A^2} = \int_{t_0}^{t} Bkdt$$

Equation 17.

$$\frac{1}{A_{samp}} - \frac{1}{A_{samp_0}} = Bkt$$

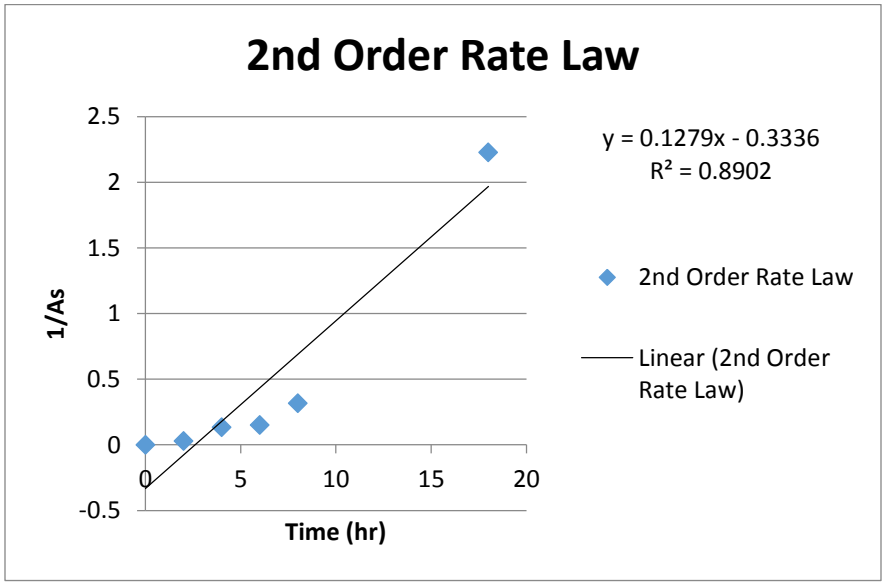

Figure 19. Second order rate law by integral method.